Raman and infrared study of nanostructured materials

Z. D. Dohčević-Mitrović, M. Šćepanović, I. Hinić,
M. Grujić-Brojčin, G. Stanišić and Z. V. Popović

Institute of Physics, Pregrevica 118, 11080 Belgrade, Serbia and Montenegro

Abstract. Nanophase materials recently gained considerable attention owing to their unique physical, mechanical and chemical properties. Raman and infrared (IR) spectroscopies are powerful optical techniques for the characterization of these materials, providing an information on chemical bond arrangements and short-range order in crystalline and amorphous nanophases. Grain size, local heating, non-stoichiometry and pressure effects lead to a frequency shift, asymmetry and broadening of the Raman lines while from IR spectra it is possible to get an information about the grain size, porosity and chemical reactions occurring at the nanoparticle surface. This paper presents a short overview of information extracted from Raman spectra of nanomaterials (TiO_2, Ge, Si, CeO_2) while the effective medium theory was used to interpret the effects of polycrystallinity and island-structure character of nanoparticles in the IR spectra of TiO_2 nanopowders.

INTRODUCTION

Nanoscience has become one of the most intensely studied areas of research over the last few decades. The interest in nanocrystalline materials is motivated by the fact that the small grain sizes give unique physical, mechanical and chemical properties which are different from their coarse-grained counterparts.

Many techniques exist for the fabrication of nanometer scale materials, including molecular beam epitaxy (MBE), metal-organic chemical vapor deposition (MOCVD), laser pyrolysis of gas phase reactants, pulsed laser deposition (PLD), sol-gel methods, sputtering and wet chemical synthesis [1-4]. Our ability to understand and manipulate materials of such small dimensions has been facilitated by advances in surface and subsurface imaging techniques such as scanning tunneling microscope (STM), atomic force microscope (AFM), near-field scanning optical microscope (NSOM), and the scanning transmission electron microscope (STEM), that have allowed imaging of nanostructured materials by providing resolutions down to a few Angstroms. Among the various techniques used to properly describe nanoscale properties Raman and infrared spectroscopies (IR) come to be of significant importance for characterization and determination of vibrational properties of nanomaterials. In this paper we gave a short overview of information extracted from Raman spectra of different nanooxide materials like anatase TiO_2 and CeO_2, as well as nanocrystalline materials like Si and Ge. From IR spectra it is possible to get an information about the grain size, porosity and chemical reactions occurring at the nanoparticle surface. Analyzing the reflectivity

spectra of anatase TiO_2 nanopowders, different from its bulk counterpart, it was evident that for proper determination of the nanocomposite dielectric function the use of the well-known classical-oscillator and factorized form of the dielectric function are insufficient [5]. It was necessary to use effective-medium theory to interpret the effects of polycrystallinity and island-structure character of TiO_2 nanoparticles.

RAMAN SPECTROSCOPY OF NANOSTRUCTURED MATERIALS

Significant information can be extracted from the peak position shift and bandshape of the Raman mode in nanomaterials. Several factors can contribute to the changes in the Raman peak position and linewidth with respect to the bulk materials like phonon confinement, strain, defects, broadening associated with the size distribution and the local heating of the sample during the measurements.

When the finite size effects are present, phonons are confined in space and the breakdown of the phonon momentum selection rule q≈0 (valid for ordered systems) will allow the contribution of optical phonons over the Brillouin zone to the first order Raman spectra. The weight of the off-center phonons increases as the crystal size decreases and the phonon dispersion causes an asymmetrical broadening and the shift of the Raman peaks. There are several phonon-confinement models frequently used for interpreting the frequency shift and broadening presented in the Raman spectra of nanomaterials [6-8]. According to them, for spherical nanoparticles of a diameter L and first-order scattering resulting Raman intensity I(ω) is a superposition of Lorentzian contributions over the whole Brillouin zone attenuated by a finite crystal size factor exp ($-q^2L^2 / 8\beta$):

$$I(\omega,L)=\int \frac{\exp(\frac{-q^2L^2}{8\beta})}{\{\ \omega-[\omega_i(q)+\Delta\omega_i(q,L)]\ \}^2+(\Gamma/2)^2}d^3q \qquad (1)$$

where $\omega_i(q)$ is the phonon dispersion curve for the selected mode, Γ is the Raman mode linewidth at room temperature, and for the time being $\Delta\omega_i(q,L)=0$. All of above mentioned models used a Gaussian weighting function to localize the phonon wavefunction within the grain boundary. In the Richter phonon-confinement model β=1 in Eq. (1) [6] while in the alternative Campbell model [7], the phonons are spatially confined even more strongly and $\beta = 2\pi^2$. Brillouin zone is considered to be spherical and the phonon dispersion curve is assumed to be isotropic. In Fig. 1 are presented measured spectra of the Raman most intensive mode of nanocrystalline Ge films for different particle size where the effect of downshift and broadening of the Raman mode with decreasing particle size is evident regarding the crystalline sample (c-Ge). In Fig. 2 are presented the measured Raman spectra of F_{2g} symmetry mode in CeO_2 nanopowders and in a single crystal. The evident red shift and broadening of the Raman line is presumably due to the size effects [9].

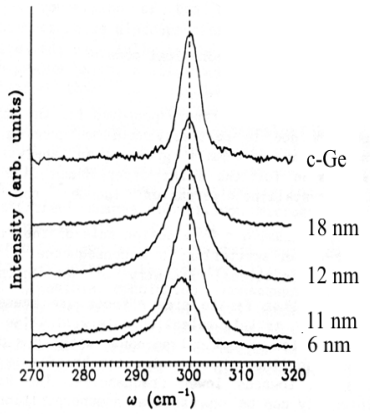

FIGURE 1. Raman spectra of nano Ge films with various particle size and the spectra of crystalline Ge (c-Ge) [8].

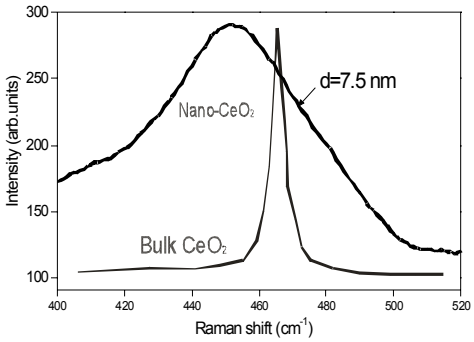

FIGURE 2. Raman spectra from nano-CeO_2 and bulk material showing size-dependant changes in the peak position and line shape [9].

The lack of use of only phonon-confinement models in interpreting Raman spectra is their incapability to describe well the asymmetric broadening of the phonon modes in Raman spectra. This broadening could be explained by introducing a Gaussian size distribution function with a mean value $\overline{L}$ and standard deviation σ for the spherical particles. In that case Raman intensity would be proportional to [8]:

$$I(\omega)= \int_0^{2\pi/a} f(q)\exp[-q\overline{L}\, f(q)/4\pi]^2 d^3q/[\omega-\omega(q)]^2+(\Gamma/2)^2 \qquad (2)$$

where $f(q) = (1+\sigma^2q^2/8\pi^2)^{-1/2}$. In Fig. 3 are presented calculated Raman spectra of Ge nanocrystalline films (nc-Ge) using equation (2) for different σ values. The mean grain size of particles is $\overline{L}$ = 10 nm. The curve with σ=0 was obtained using Campbell phonon-confinement model [7].

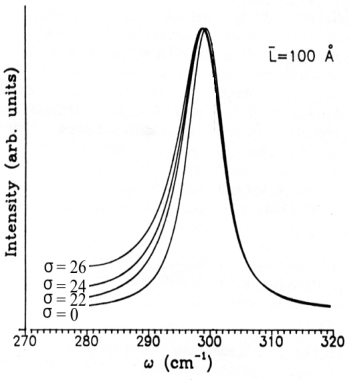

FIGURE 3. Calculated Raman line of a nc-Ge for different σ values together with the curve σ=0 obtained by Campbell model [8].

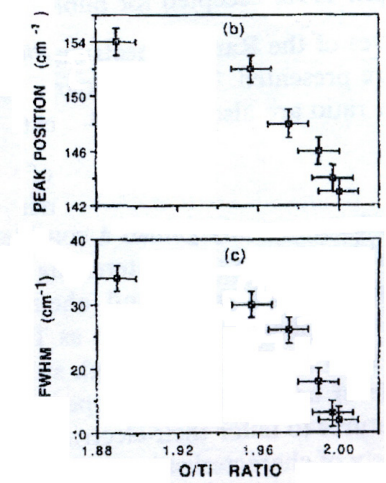

FIGURE 4. Variation with O/Ti ratio of the peak position and full width of the E_g anatase mode [10].

As can be seen from Fig. 3, the line position is determined essentially by the mean grain size $\overline{L}$ while the asymmetry in the curve is dominated by the dispersion in the grain sizes.

Defect structures within nanomaterials strongly affect the Raman spectrum. In nanooxide materials like, for example TiO_2, oxygen vacancies at the surface can produce large blueshift and broadening of E_g anatase mode as it is shown in Fig. 4 [10].

Another important effect that influence on the position and phonon line shape of the first-order Raman modes is the increase of the local temperature during the measurements. In order to take into account the temperature change it is necessary to include anharmonic coupling between phonons in disorder scattering models (Eq. (1)) through the three and four–phonon decay processes [11]:

$$\omega(q,T) = \omega(q) + \Delta T\ ,\ \Delta T = C\left[1 + \frac{2}{e^{\hbar\omega/2k_BT} - 1}\right] + \mathrm{D}\left[1 + \frac{3}{e^{\hbar\omega/3k_BT} - 1} + \frac{3}{\left(e^{\hbar\omega/3k_BT} - 1\right)^2}\right] \quad (3)$$

$$\Gamma(T) = A\left[1 + \frac{2}{e^{\hbar\omega/2k_BT} - 1}\right] + B\left[1 + \frac{3}{e^{\hbar\omega/3k_BT} - 1} + \frac{3}{\left(e^{\hbar\omega/3k_BT} - 1\right)^2}\right] \quad (4)$$

where A, B, C, D are anharmonic constants. Temperature dependence of T_{2g} phonon frequency in silicon nanograins (squares) is shown in Fig. 5 [12]. The calculated phonon frequencies for 10 nm-Si nanograins with included anharmonicity in phonon-confinement models (Eq. (1)), are presented with a full line. It is obvious from Fig. 5 that the calculated frequencies trace well the experimental ones. It is worth mentioning that it was not possible to describe well the shift and broadening of the T_{2g} mode of Si nanograins without anharmonicity effects.

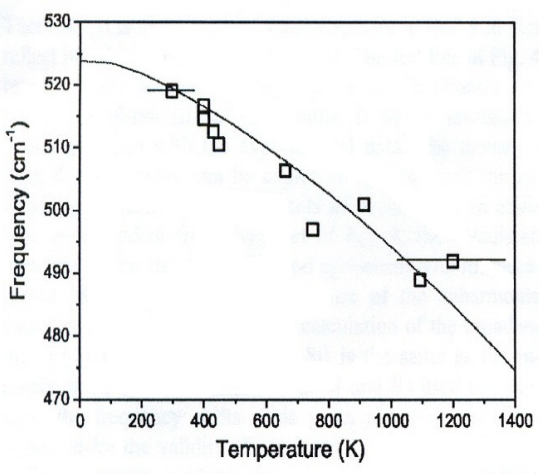

FIGURE 5. Temperature dependence o the T_{2g} phonon mode in 10 nm-S nanograins. The squares are experimenta values while the full line presents th calculated values including phono confinement and anharmonicity effect [12].

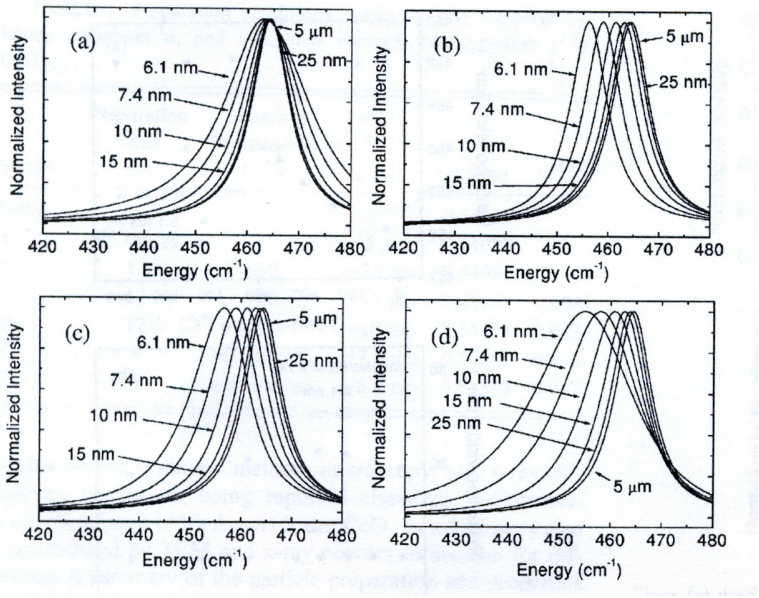

FIGURE 6. Calculated Raman spectra of CeO_2 for various nanoparticle sizes, for (a) only confinement effects, (b) average strain, (c) only inhomogeneous strain and (d) the combination of confinement and inhomogeneous strain [14].

In nanomaterials large fraction of atoms reside in the surface and the surface energy makes more contribution to the total energy than in the bulk materials. This surface tension may exert a radial pressure on the nanocrystal, the smaller the crystallite the larger is the radial pressure. The changes in the lattice parameter ($\triangle a$) can be related to a surface pressure through the Laplace Law [13]. These changes can affect the Raman peak position. Therefore, Raman mode centred at ω_i changes by [14]:

$$\triangle\omega_i(q, L) = -3\gamma_i(q)\omega_i(q)\times[\triangle a/a_0] \quad (5)$$

where $\triangle a/a_0 \sim 1/L^2$, γ_i is a mode Grüneisen parameter and a_0 is a lattice parameter of the bulk material.

The dispersion in particle size produces a dispersion of lattice parameters and leads to the inhomogeneous strain. The final effect is asymmetric broadening and a shift of Raman mode. In Fig. 6 are summarized effects due to the confinement and strain as well as their combination on the Raman spectra of CeO_2 nanoparticles.

INFRARED SPECTROSCOPY OF NANOSIZED MATERIALS

The analysis of nanosized particles by Fourier transform infrared (FTIR) spectroscopy brings information on the bulk, and surface. From the infrared spectrum it is possible to obtain information about the interatomic bonds constituting the bulk, the chemical nature of the surface bonds and surface groups, the possible presence of contaminating species on the surface and the surface reactions.

Dielectric function obtained from experiment can give an insight into the nanostructure of the materials. In principle one can deduce the value of the microscopic parameters of a noncrystalline solid comparing the measured IR spectra with simulated ones. Furthermore, structural information concerning the shape, orientation, and distribution of the individual vibrating units can also be obtained [15].

In this work we have analyzed the infrared reflectivity spectra of anatase TiO_2 nanopowders in order to determine properly the nanocomposite dielectric function.

Dielectric function of anatase single crystal TiO_2 was obtained from polarization-dependent far-infrared reflectivity measurements using factorized form for dielectric function [16]. These results were used to explain infrared reflectivity spectra of titania nanoparticles pressed into pellets. Because of the polycrystalline and porous character of the titania nanoparticles effective-medium theories (appropriate for composites) were used, along with the anatase dielectric functions, to interpret well the experimental results [17].

FTIR reflectivity spectra of two laser synthesized anatase TiO_2 nanopowders with specific surface area (S_{BET}) of 84 and 110 m^2/g in the range 100-1500 cm^{-1} are presented in Fig. 7. SEM measurements have shown that mean grain size of the first powder was about 70 nm and about 30 nm of the second one. We have analyzed these reflectivity spectra with a combination of:

(a) effective medium theories;
(b) bulk crystal data;
(c) polycrystalline character of nanopowder;
(d) porosity of nanopowder.

The polycrystalline character of nanopowder is implemented by determining the dielectric function $\varepsilon_{pc}(\omega)$ from:

$$\frac{1}{3}\left(\frac{\varepsilon_{||}-\varepsilon_{\mathrm{pc}}}{\varepsilon_{||}+2\varepsilon_{\mathrm{pc}}}\right)+\frac{2}{3}\left(\frac{\varepsilon_{\perp}-\varepsilon_{\mathrm{pc}}}{\varepsilon_{\perp}+2\varepsilon_{\mathrm{pc}}}\right)=0 \qquad (6)$$

where $\varepsilon_{||}(\omega)$ and $\varepsilon_{\perp}(\omega)$ are the dielectric functions of single crystal anatase TiO_2 for two different polarizations with respect to the c axis ($E\|c$ and $E\perp c$). Equation (6) was deduced from Bruggeman effective-medium model [18]. It assumes the pellet to be a nanocomposite of two fictitious isotropic materials, one having dielectric function $\varepsilon_{||}(\omega)$ and other having dielectric function $\varepsilon_{\perp}(\omega)$, with volume fractions 1/3 for the first and 2/3 for the second material.

As nanophase titania is a porous material with relatively great specific surface we included a porosity of nanopowder in modeling of its dielectric function. Best agreement between calculated and experimental results was obtained by generalized Bruggeman effective-medium model [19] which introduces the effect of pore shape by using the adjustable depolarization factor L_j for ellipsoidal voids (L_j=1/3 for spherical cavities and $1/3<L_j<1$ for prolate spheroidal cavities):

$$\left(\frac{\varepsilon_{\mathrm{pc}}-\varepsilon_{\mathrm{eff}}}{\varepsilon_{\mathrm{eff}}+L_j\left(\varepsilon_{\mathrm{pc}}-\varepsilon_{\mathrm{eff}}\right)}\right)f_{\mathrm{TiO_2}}+\left(\frac{\varepsilon_{\mathrm{air}}-\varepsilon_{\mathrm{eff}}}{\varepsilon_{\mathrm{eff}}+L_j\left(\varepsilon_{\mathrm{air}}-\varepsilon_{\mathrm{eff}}\right)}\right)f_{\mathrm{air}}=0, \qquad (7)$$

The nanopowder with dielectric function ε_{eff} is assumed to be a nanocomposite of polycrystalline TiO_2 (with dielectric function ε_{pc} calculated from Eq. (6) and air (ε_{air}=1). The volume fractions of titania and air are $f_{\mathrm{TiO_2}}$ and f_{air}, respectively. Note that f_{air}=1- $f_{\mathrm{TiO_2}}$ expressed in percents corresponds to macroscopic value of

nanopowder porosity. IR reflectivity spectra, shown in Fig. 7 by solid lines, are obtained from calculated dielectric function ε_{eff} using Eq. (7) for several values of f_{TiO_2} ($0.55<f_{TiO_2}<0.75$) and L_j=0.655. It's evident from experimental and corresponding fitted spectra that for TiO_2 nanopowder with higher S_{BET} value (smaller particle size) the value of f_{air} is bigger. This is in agreement with results obtained for TiO_2 nanoparticles by the other methods [20]. This example is a good illustration of possibility of making a relation between IR spectra features and size and shape of grains and pores in nanomaterials.

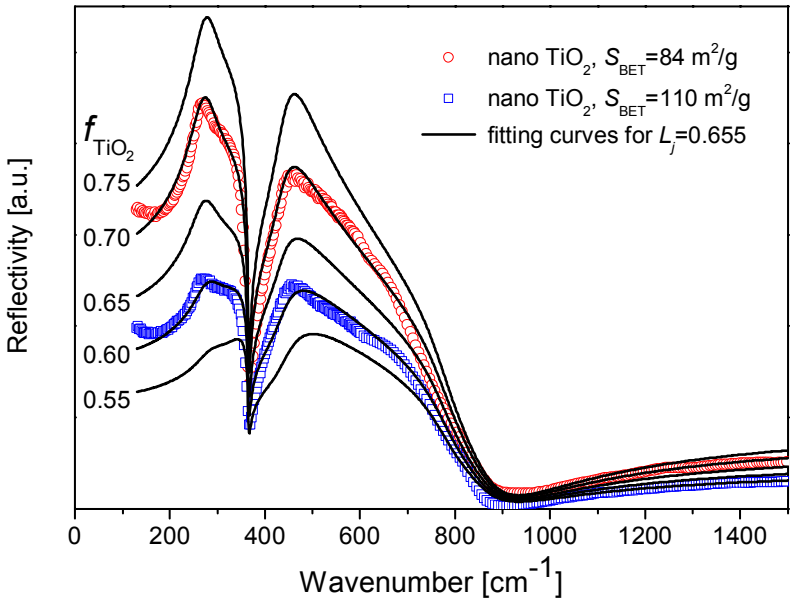

FIGURE 7. Calculated (solid lines) and experimental (circles and squares) IR spectra of anatase TiO_2 nanopowders.

CONCLUSION

In this work we have demonstrated that Raman and infrared spectroscopies are very useful optical techniques for the characterization of nanocrystalline materials. From the shift and change of the lineshape of the Raman mode it is possible to get the information about the size and shape of the nanoparticles, the nanomaterial stoichiometry and about the effects of surface states that contribute appreciably to the position and shape of the Raman mode. From the IR spectra it is possible to get the information about the grain size, porosity, nature of the surface bonds and reactions occurring at the nanoparticle surface.

ACKNOWLEDGMENTS

This work is supported by SMSEP under the project No. 1469.

REFERENCES

1. HeatJ. R., Shiang J.J. and Alivisatos A.P., *J. Chem. Phys.* **101,** 1607-1610 **(**1994).
2. Kim S. Y., Yu J. H. and Lee J. S., *Nanostructured materials* **12**, 471-474 (1999).
3. Musci M., Notaro M., Curcio F., Casale C. and De Michele G., *J. Mater. Res.* **7**, 2846-2852 (1992).
4. Harizanov O., Harizanova A., *Solar Energy Materials & Solar Cells* **63**, 185-195 (2000).
5. Gervais F., *Infrared and Millimeter Waves* **8**, 279-339 (1983).
6. Richter H., Wang Z. P. and Levy L., *Solid State Comm*. **39**, 625-629 (1981).
7. Campbell I. H. and Fauchet P. M., *Solid State Comm.* **58**, 739-741 (1986).
8. Santos D. R. and Torriani I. L., *Solid State Comm*. **85**, 307-310 (1993).
9. Z. Dohčević-Mitrović et al., (in preparation).
10. Parker J. C. and Siegel R. W., *Appl. Phys. Lett.* **57**, 943-945 (1990).
11. Balkanski M. Wallis R. F. and Haro E., *Phys. Rev. B* **28**, 1928-1934 (1983).
12. Konstantinović M. J., Bersier S., Wang X., Hayne M., Lievens P., Silverans R. E. and Moshchalkov V. V., *Phys. Rev. B* **66**, 161311-1-161311-4 (2002).
13. Tolbert S. H. and Alvisiatos A. P., *Annu. Rev. Phys. Chem.* **46**, 595-625 (1995).
14. Spanier J. E., Robinson R. D., Zhang F., Chan S. W. and Herman I. P., *Phys. Rev. B* **64**, 245407-1-245407-7 (2001).
15. Scarel, G., Hirschmugl, C. J., Yakovlev, V. V., Sorbello, R. S., Aita, C. R., Tanaka, H. and Hisano, K., *J. Appl. Phys.* **91**, 1118-1128 (2002).
16. Gonzalez, R. J., Zallen, R. and Berger, H., *Phys. Rev. B*, **55** 7014-7017 (1997).
17. Grujić-Brojčin, M., Šćepanović, M., Dohčević-Mitrović, Z., Hinić, I., Stanišić, G., Popović, Z. V., Kongres fizičara Srbije i Crne Gore, Petrovac na moru, 3-5. jun 2004, pp. 4-57–4-60.
18. Bruggeman, D. A. G., *Ann. Phys.* **24**, 636- (1935).
19. Spanier, J. E., Herman, I. P., *Phys. Rev. B* **61**, 10437-10450 (2000).
20. Nakade, S., Saito, Y., Kubo, W., Kitamura, T., Wada Y., and Yanagida, S., *J. Phys. Chem. B* **107**, 8607-8611 (2003).